PCCP

Accepted Manuscript

ROYAL SOCIETY OF CHEMISTRY

www.rsc.org/pccp

Waveguide-coupled Directional Raman Radiation for Surface Analysis

Chen Chen, Jin-yang Li, Li Wang, Dan-Feng Lu, Zhi-Mei Qi*
State Key Laboratory of Transducer Technology, Institute of Electronics, Chinese Academy of Sciences, Beijing 100190, P. R. China
**Corresponding author: zhimei-qi@mail.ie.ac.cn*

Abstract: Kretschmann-type waveguide structures, including Plasmon Waveguide (PW) and Resonant Mirror (RM), have been applied to interfacial Raman spectroscopy because of the following unique features: (1) unlike the classic surface enhanced Raman scattering (SERS) substrates made of either gold or silver, both PW and RM can be prepared with a large variety of inexpensive materials; (2) the field enhancement factors with these structures can be theoretically predicted and experimentally controlled, which enables us to manipulate the surface Raman sensitivity with high repeatability; (3) the use of transverse electric (TE) and transverse magnetic (TM) modes for Raman excitation allows us to evaluate the orientation of target molecules immobilized on the waveguide surface; (4) the unwanted impact of noble metals on the Raman fingerprints of target molecules, which is often observed with conventional SERS substrates, can be avoided with the use of dielectric waveguides. In this paper, the guided-mode-coupled directional Raman emission that is an additional important feature of the waveguide Raman technique was theoretically investigated based on the optical reciprocity theorem combined with the Fresnel equations. The simulation results indicate that the directional Raman emission from a dipole located within the field confinement and penetration depth of a guided mode depends on both the dipole's orientation and its distance from the waveguide surface. Raman light from the TE-oriented dipoles is launched into the prism coupler at the TE-mode resonance angle and that from the non-TE-oriented dipoles propagates at the TM-mode resonance angle. The intensity of the guided-mode-excited Raman signal propagating at the mode resonance angle is proportional to the fourth power of the mode field (E^4) at the dipole's depth from the waveguide surface. This means that the guided-mode-excited and guided-mode-coupled directional Raman spectroscopy has a detection depth as small as a quarter of the evanescent-field penetration depth, indicating the excellent surface selectivity of this technique. The directional Raman emission also facilitates high-efficiency signal collection compared with conventional SERS. It is worth noting that Raman light from the dipoles confined in the core layer of a single-mode waveguide can be simultaneously coupled into both the guided mode and the substrate mode, especially the Surface Plasmon Resonance (SPR) mode for PW.

Keywords: Directional Raman emission; Plasmon waveguide; Resonant mirror; Excellent surface selectivity; High-efficiency Raman collection

Surface Enhanced Raman Spectroscopy (SERS) has attracted significant attention in the past decade due to its molecular recognition and label-free nondestructive detection capabilities and its ultrahigh sensitivity as well as the rapid development of nanotechnologies [1-4]. However, SERS has several intrinsic shortcomings that preclude its widespread applications in surface and interface analyses. First of all, only a few kinds of noble metals, such as gold and silver, can offer SERS substrates a large field enhancement factor, making the availability of materials very limited [5]; Secondly, to achieve the Localized Surface Plasmon Resonance (LSPR) effect that is responsible for field enhancement, the metallic surface of SERS substrates must be roughened in nanoscale but the nanoscale architectonics is complicated and less reproducible [6]; Thirdly, Raman light from the target molecules attached to the SERS substrate is non-directional, resulting in low signal collection efficiency [7]; Last but not the least, the interaction between target molecules and the metallic surface of SERS substrates often brings about the undesirable influence on the Raman fingerprints of the target molecules [8].

In order to address the issues mentioned above, many researchers have refocused their attention to flexible multilayer substrates with smooth flat surfaces for Raman spectroscopy with the Total Internal Reflection (TIR) excitation method [9]. The very earlier version of this kind of Raman substrates is actually surface plasmon resonance (SPR) sensor chips that can provide a moderate but repeatable field enhancement based on the propagating surface plasmon mode [10-13]. The reproducibility of Raman spectroscopy was indeed improved with the use of SPR chips. However, the noble metals indispensable to SPR chips can still cause the unwanted impact on the Raman fingerprints of target molecules. To overcome this shortcoming, the use of Plasmon Waveguide (PW) for Raman spectroscopy was proposed recently [14]. PW contains a metal film as the buffer layer and an upper dielectric film as the core layer, and it can prevent the direct contact of target molecules with the metal component. Most recently, our group successfully implemented the surface Raman spectroscopy using Resonant Mirror (RM) [15]. RM is similar in structure to PW but does not contain the metal layer. Owing to no absorption of light by a metal layer, RM can provide a higher field enhancement factor than PW. Unlike the SPR chips that operate only in the TM mode, both PW and RM enable to work in either the TM mode or the TE mode: this is very important for investigating the spatial orientation of target molecules bound to the waveguide surface [16]. The SPR, PW and RM structures have the two common features: one is the simultaneous surface sensing and surface Raman spectroscopy and the other is the directional Raman emission called the reverse Kretschmann configuration. The first common feature makes them able for precise measurements of chemical and biological measurands. Although their second common feature has more important implications for the surface and interface analyses, it has not yet attracted considerable interest from academic and industrial communities. The collection of non-directional Raman light from the air-clad side, despite of its low efficiency and inferior surface selectivity relative to the directional Raman detection approach, is still routinely used in the waveguide Raman spectroscopy measurements [17-21]. The reason responsible for this embarrassing situation is the lack of deep theoretical understanding of the directional emission characteristic for the waveguide Raman spectroscopy.

The previous investigations into the directional Raman/fluorescence emission phenomenon are exclusively focused on the SPR structure [22, 23]. In this work, the guided-mode-coupled directional Raman emission properties for the PW and RM structures are systematically analyzed based on the optical reciprocity theorem combined with the Fresnel equations. The angular

distributions of Raman power density from the molecular dipole located at different positions in the mode-field occupying space (above, on and in the core layer of a waveguide) are calculated. The interesting and meaningful simulation results are obtained, which are very helpful for us to understand the directional Raman emission characteristic of the waveguide Raman technique. The optical reciprocity theorem as the basis for simulation modeling was briefly described below.

1. Optical reciprocity theorem

The optical reciprocity theorem indicates that the electric field $\mathbf{E}_1$ generated at the point Q_2 by a dipole $\mathbf{p}_1$ ($\mathbf{p_1} = p_1\mathbf{e_1}$ with $\mathbf{e_1}$ denoting the oscillation direction) at the point Q_1 and the electric field $\mathbf{E}_2$ yielded at the point Q_1 by a dipole $\mathbf{p}_2$ ($\mathbf{p_2} = p_2\mathbf{e_2}$) at the point Q_2 are related to each other through eq. (1) [24]:

$$\mathbf{p}_1 \cdot \mathbf{E}_2 = \mathbf{p}_2 \cdot \mathbf{E}_1 \tag{1}$$

If the distance (r) between the points Q_1 and Q_2 is sufficiently large and there are no scatterers between them, $\mathbf{E}_2$ can be considered as a plane wave propagating in the opposite direction to $\mathbf{r}$ ($\mathbf{r}$ is a vector from Q_1 to Q_2) [7], and the electric-field amplitude (E_P) of this plane wave can be expressed by eq.(2):

$$E_p = \frac{\omega^2 p_2 e^{ik_m r}}{4\pi\varepsilon_0 c^2 r} \tag{2}$$

Where ω is the angular frequency of oscillation of $\mathbf{p}_2$, $k_m = (\omega/c)n_m$ with n_m denoting the refractive index of the medium in which the plane wave propagates.

If there are scatterers between the points Q_1 and Q_2, $\mathbf{E}_2$ is no longer a plane wave and it can be replaced by the local field ($\mathbf{E}_{loc}$) at the point Q_1 excited by the plane wave. By substituting $\mathbf{E}_2$ in eq. (1) with $\mathbf{E}_{loc}$, one can deduce the following equation:

$$\mathbf{e}_2 \cdot \mathbf{E}_1 = \frac{p_1}{p_2}\mathbf{e}_1 \cdot \mathbf{E}_{loc} = \frac{E_p}{p_2} p_1 \frac{\mathbf{e}_1 \cdot \mathbf{E}_{loc}}{E_p} = \frac{\omega^2 p_1 e^{ik_m r}}{4\pi\varepsilon_0 c^2 r} \frac{\mathbf{e}_1 \cdot \mathbf{E}_{loc}}{E_p} \tag{3}$$

Assuming $\mathbf{p}_2 // \mathbf{E}_1$ and setting $EF_{field} = \mathbf{e}_1 \cdot \mathbf{E}_{loc}/E_p$ (EF_{field} represents the field enhancement factor induced by scatterers), eq. (3) can then be simplified as:

$$E_1 = \frac{\omega^2 p_1 e^{ik_m r}}{4\pi\varepsilon_0 c^2 r} EF_{field} \tag{4}$$

E_1 is the far-field strength generated by $\mathbf{p}_1$. Based on the Poynting's theorem, the power density radiated by $\mathbf{p}_1$ along the direction $\mathbf{r}$ (*i.e.*, Poynting vector) can be determined using eq. (5):

$$\langle \mathbf{S}_1 \rangle = \frac{n_m \varepsilon_0 c}{2} E_1^2 \mathbf{e}_r = \frac{n_m \omega^4 p_1^2}{32\pi^2 \varepsilon_0 c^3 r^2} EF_{field}^2 \mathbf{e}_r \tag{5}$$

Where $\mathbf{e}_r$ is the unit vector of $\mathbf{r}$. Given the total radiation power of the dipole $\mathbf{p}_1$ is P = 1W, then the square of the dipole moment amplitude can be determined as $p_1^2 = (12\pi\varepsilon_0 c^3/\omega^4)$ W from the formula $P = (\omega^4 p_1^2)/(12\pi\varepsilon_0 c^3)$ [25]. By substituting $p_1^2 = (12\pi\varepsilon_0 c^3/\omega^4)$ W in eq. (5) and setting r = 1m, the following equation is obtained, which can be used to determine the angular distribution of the power density in the far-field region (r = 1m) for $\mathbf{p}_1$:

$$\mathbf{P}(\mathbf{r}) = \frac{3n_m}{8\pi} EF_{field}{}^2 \mathbf{e}_r (\mathrm{W/m^2}) \quad (6)$$

Eq. (6) indicates that the power density emitted in the direction **r** from a molecular dipole can be obtained by calculating the field enhancement factor at the dipole's location induced by the incident plane wave propagating in the opposite direction to **r**. In the case of $EF_{field} = 1$, the power density emitted from a dipole in free space has the maximum of $\mathbf{P}(\mathbf{r})=0.12\mathrm{W/m^2}$ in the direction normal to the orientation of the dipole. It has been recognized that the Kretschmann-type multilayer structures, including SPR and PW and RM, have the significant field-enhancement effect. Moreover, the field enhancement factor EF_{field} with these structures can be accurately calculated based on the Fresnel equations. This suggests that the use of these structures for either Raman or fluorescence spectroscopy enables us to theoretically predict the angular distribution of the power density emitted from the target molecules. In the previous papers, the angular distribution of the Raman (or fluorescence) power density with the SPR structure was simulated and the reverse Kretschmann configuration theoretically predicted has been verified experimentally [26]. This work focuses on the cases with PW and RM. It is worth noting that the radiation patterns obtained below are not related to the excitation method and only involve the mode-resonance induced directional emission.

2. Radiation pattern of Raman dipole with PW

2.1. Raman dipole located above the core layer

Figure 1 schematically shows the single-mode plasmon waveguide used for simulation. The PW consists of a glass prism coupler with refractive index of $n_P = 1.76$, a 50-nm-thick gold layer with complex refractive index of 0.143+ i4.799, a dielectric core layer with thickness of D_w = 300nm and refractive index of $n_w = 1.454$, and the air clad of $n_c = 1$. A molecular dipole is assumed to be located at a distance Z from the gold/core interface and its radiation wavelength in vacuum is given to be λ = 532nm. From Fig. 1 it is seen that the Raman radiation from the dipole can be classified into two cases: (1) the Raman radiation goes into the air clad, and in this case, the field enhancement factor is written as $EF_L^{\uparrow}(\theta, Z)$; (2) the Raman radiation enters the prism side and the corresponding field enhancement factor is denoted as $EF_L^{\downarrow}(\theta, Z)$. Both $EF_L^{\uparrow}(\theta, Z)$ and $EF_L^{\downarrow}(\theta, Z)$ are a function of the angle θ between the radiation direction and the PW surface normal.

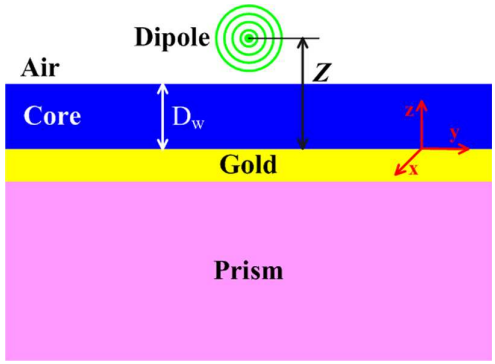

Fig. 1 Schematic diagram of a PW with the core layer thickness of D_w and a Raman dipole at a distance Z from the surface of the lower gold layer. In the case of a RM, the lower gold layer is replaced with a low-index dielectric film.

As long as the orientation of a dipole in the space occupied by the PW mode is given, the power density radiated from this dipole can be readily obtained as a function of the angle θ. To do this, θ dependence of the EF_{field} at the dipole's location for the PW is first calculated using the Fresnel equations.

The Raman dipole with the orientation parallel to the x axis (namely, the TE orientation) was first considered. In this case, the TE-polarized field enhancement factor with the PW is calculated using eqs. (7) and (8):

$$EF_{L,x}{}^{\uparrow}(\theta, Z) = \left|1 + r_s{}^{\uparrow} e^{2ik_3(Z-D_w)\cos\theta}\right| \quad (7)$$

$$EF_{L,x}{}^{\downarrow}(\theta, Z) = \left|t_s{}^{\downarrow} e^{ik_3(Z-D_w)\cos\theta_r}\right| \quad (8)$$

where $r_s{}^{\uparrow}$ stands for the TE-polarized electric field reflection coefficient at the core/air interface with air-clad side incident plane wave, $t_s{}^{\downarrow}$ represents the TE-polarized electric field transmission coefficient from the prism/gold interface to the core/air interface, θ is the incident angle (here θ is defined as same as that mentioned above), θ_r is the corresponding refraction angle in air and k_3= $2\pi/\lambda$ with λ denoting the wavelength in vacuum [27]. With the $EF_L{}^{\uparrow}(\theta, Z)$ and $EF_L{}^{\downarrow}(\theta, Z)$ determined from eqs. (7) and (8), respectively, the angular distribution of Raman power density radiated from the dipole located at Z and oriented parallel to the x axis can be achieved. Fig. 2(a) and 2(b) display the simulation results for the x-oriented dipole located at $Z=D_w$ and $Z=D_w+\lambda$, respectively. According to Fig. 2(a), most of the radiation power from the dipole located on the PW surface is transferred to the TE resonance mode in the PW to be finally coupled into the prism side at the TE-mode resonance angle (θ_s=47.43°). The Raman power density radiated at this resonance angle is calculated to be 11.84W/m^2, 98 times larger than the maximum power density of 0.12W/m^2 for the dipole radiation in free space. When the dipole is located at a distance of λ apart from the PW surface, more than 99% of the radiation power goes into the air clad and no obvious directional emission appears [see Fig. 2(b)]. The comparison of Figs. 2(a) and 2(b) clearly indicates that the directional emission effect with the PW is closely related to the distance from the dipole to the PW surface: larger the distance, weaker the directional emission effect. Fig. 2(c) shows the TE-mode-coupled directional power density calculated as a function of the distance from the dipole to the PW surface (Z >0.3μm). The power density is exponentially decreased from 11.84 W/cm^2 down to almost zero with moving the dipole from Z=0.3μm to Z≈0.7μm. The findings reveal that the use of PW for Raman spectroscopy can lead to a good depth resolution. To explain the depth resolution of this technique, we introduce "the detection depth" that is actually a special distance from the dipole to the PW surface. When the dipole is located at this special distance, the directional power density from it decreases down to 1/e of the value (11.84 W/m^2) for the same dipole on the PW surface (Z=0.3μm). On the base of the waveguide theory, one can easily deduce that the above-defined detection depth is half as large as the penetration depth of the evanescent field. In the case of 532 nm wavelength, the field penetration depth is about 200 nm, and thus the detection depth for the guided-mode-coupled directional Raman spectroscopy is approximately 100 nm. The findings indicate that the PW based directional Raman spectroscopy has a good surface selectivity. It is worth noting that the detection depth can be further decreased by combining the guided-mode excitation of Raman signal with the guided-mode-coupled directional Raman emission. The detection depth for the guided-mode-excited and guided-mode-coupled directional Raman spectroscopy is merely a quarter of the field penetration

depth.

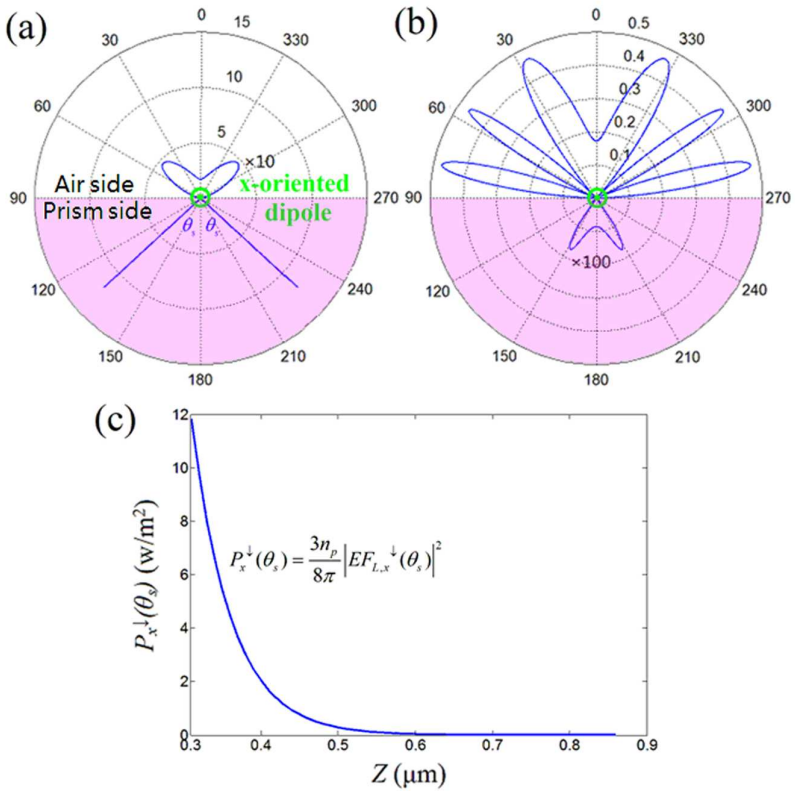

Fig. 2 Angular distribution of Raman power density from the x-oriented dipole located at a distance of (a) $Z=D_w$ (*i.e.*, on the surface of the core layer) and (b) $Z=D_w+\lambda$ (*i.e.*, a wavelength apart from the surface); (c) Power density radiated at the TE-mode resonance angle of θ_s =47.43° as a function of the distance Z [for a clear view, the power density on the air-clad side in (a) and that on the prism side in (b) is multiplied by 10 and 100, respectively].

Different from the x-oriented dipole that emits the TE-polarized directional Raman signal, the y-oriented dipole generates directional Raman emission with the TM polarization. The above-mentioned eqs. (7) and (8), which are suitable for calculating the TE-polarized field enhancement factor, are no longer applicable to the calculation of the TM-polarized field enhancement factor. The TM-polarized field enhancement factor with the PW can be calculated using eqs. (9) and (10):

$$EF_{L,y}^{\uparrow}(\theta, Z) = \left|1 - r_p^{\uparrow} e^{2ik_3(Z-D_w)\cos\theta}\right| \cos\theta \tag{9}$$

$$EF_{L,y}^{\downarrow}(\theta, Z) = \left|t_p^{\downarrow} e^{ik_3(Z-D_w)\cos\theta_r} \cos\theta_r\right| \tag{10}$$

$r_p^{\uparrow}$ stands for the TM-polarized electric field reflection coefficient at the core/air interface with air-clad side incident plane wave and $t_p^{\downarrow}$ represents the TM-polarized electric field transmission coefficient from the prism/gold interface to the core/air interface. Fig. 3(a) and 3(b) are the simulation results with the y-oriented dipole located at $Z= D_w$ and $Z=D_w+\lambda$, respectively. According to Fig. 3(a), a majority of the radiation power from the dipole located on the PW surface is coupled to the TM resonance mode and then directionally emitted into the prism at the TM-mode resonance angle (θ_p=37.95°). The Raman power density radiated at this resonance angle

is 2.16W/m^2, 17 times larger than the maximum power density emitted in free space. When the dipole is located at a distance of λ apart from the PW surface, the power radiated into the prism can almost be neglected compared with its opponent on the air-clad side. Fig. 3(c) shows the Z dependence of the TM-mode-coupled directional power density. The power density exponentially decreases from 2.16 W/cm^2 (Z=0.3μm) down to almost zero (Z≈0.8μm). In this y-axis TM case the tail of Raman power density extends to increased z values than with the dipole oriented in the x-direction. This is because the TM resonance mode has a larger evanescent field penetration depth compared with the TE resonance mode.

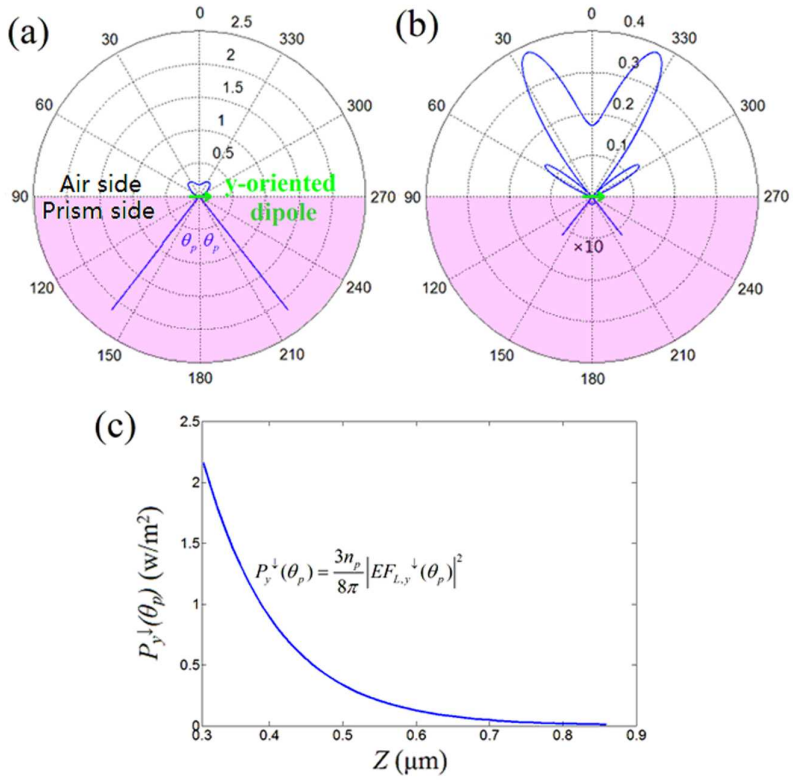

Fig. 3 Angular distribution of Raman power density from the y-oriented dipole located at (a) $Z=D_w$ and (b) $Z=D_w+\lambda$; (c) Power density radiated at the TM-mode resonance angle of θ_p=37.95^o as a function of the distance Z [the power density on the prism side in (b) is multiplied by 10 for a clear view].

When the orientation of the Raman dipole is parallel to the z-axis, it generates the directional Raman emission with the TM polarization. In this case, the field enhancement factors, $EF_L^{\uparrow}(\theta, Z)$ and $EF_L^{\downarrow}(\theta, Z)$, can be expressed by eqs. (11) and (12), respectively.

$$EF_{L,z}^{\uparrow}(\theta,Z)=\left|1+r_p^{\uparrow}e^{2ik_3(Z-D_w)\cos\theta}\right|\sin\theta \tag{11}$$

$$EF_{L,z}^{\downarrow}(\theta,Z)=\left|t_p^{\downarrow}e^{ik_3(Z-D_w)\cos\theta_r}\sin\theta_r\right| \tag{12}$$

Figs. 4(a) and 4(b) show the simulation results with the z-oriented Raman dipole located at $Z=D_w$ and $Z=D_w+\lambda$, respectively. It is seen from Fig. 4(a) that the TM-mode-coupled directional power density is 14.76W/m^2, 122 times larger than the maximum power density emitted in free space. According to Fig. 4(b), a weak directional emission can be observed when the distance increases

to $Z=D_w+\lambda$. Fig. 4(c) shows Z dependence of the directional power density from the z-oriented dipole. A comparison between Figs. 3(c) and 4(c) reveals that the TM-mode-coupled directional emission efficiency with the z-oriented Raman dipole is much higher than that with the y-oriented dipole.

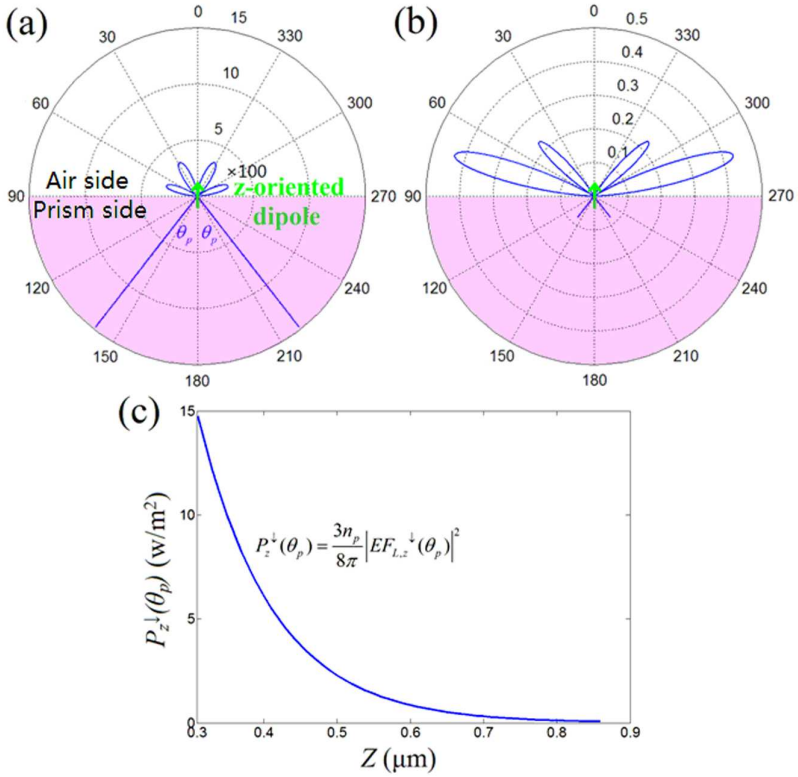

Fig. 4 Angular distribution of Raman power density from the z-oriented dipole located at (a) $Z=D_w$ and (b) $Z=D_w+\lambda$; (c) Power density radiated at the TM-mode resonance angle of θ_p =37.95° versus the distance Z [the power density on the air-clad side in (a) is multiplied by 100 for a clear view].

In the case of the dipole moment not parallel to any of the three axes, its radiation pattern should be the linear combination of the three cases mentioned above. It is clear that the coupling between the radiation power and the waveguide resonance modes is possible only when the Raman dipole is located close enough to the PW surface (with distance less than λ according to Fig. 2(c), 3(c) and 4(c)) and the coupling efficiency decreases rapidly with increasing the distance. It is worth pointing out that part of the radiation power *could* be coupled into SPR resonance mode. However, because of the large distance between Raman dipole and the gold layer, it is very weak and can safely be ignored in this case.

2.2. Raman dipole located in the core layer

When the target molecules are immobilized in the core layer of a waveguide, both the guided-mode-excited Raman radiation efficiency and the coupling efficiency between the Raman light and the guided mode can be significantly improved [19, 28, 29]. In this case, the directional Raman emission with the PW structure could be very strong. In this section, the radiation patterns for a Raman dipole located at different distances in the core layer ($0 \leq Z < D_w$) are calculated with the PW structure.

The simulation with the x-oriented Raman dipole can be carried out by considering the core layer as two independent layers separated by the dipole. Defining $t_s^{\uparrow}$ as the TE-polarized electric field transmission coefficient from the core/air interface to the prism/gold interface and defining $t_{s1}^{\uparrow}$ and $r_{s1}^{\uparrow}$ as the TE-polarized electric field transmission and reflection coefficients from the dipole-containing interface to the prism/gold interface, then the transmission coefficient from the core/air interface to the dipole-containing interface should be $t_s^{\uparrow}/t_{s1}^{\uparrow}$ and the corresponding reflection coefficient should be $(t_s^{\uparrow}/t_{s1}^{\uparrow})\cdot r_{s1}^{\uparrow}$. Consequently, the field enhancement factor $EF_L^{\uparrow}(\theta, Z)$ associated with the power radiating into the upper half space can be expressed as eq. (13). This equation also includes the case with the power radiating into the lower half space [*i.e.*, $t_{s1}^{\downarrow}$ and $r_{s1}^{\downarrow}$ and $EF_L^{\downarrow}(\theta, Z)$].

$$EF_{L,x}^{\downarrow,\uparrow}(\theta,Z)=\left|\frac{t_s^{\downarrow,\uparrow}}{t_{s1}^{\downarrow,\uparrow}}(1+r_{s1}^{\downarrow,\uparrow})\right| \tag{13}$$

Combing eq. (13) with eq. (6), the angular distribution of Raman power density from the x-oriented dipole can be obtained. Fig. 5(a) shows the TE-mode-coupled directional Raman power density as a function of the distance Z. The largest power density, which is 30.36W/m^2, is now 252 times larger than the maximum power density emitted in free space. This value is achieved with Z = 0.185μm, radiation pattern of which is given by Fig. 5(b). It is consistent with the fact that the largest electric field of the TE resonance mode must be located in the core layer and the directional Raman power density can be larger than that with dipole located on the PW surface.

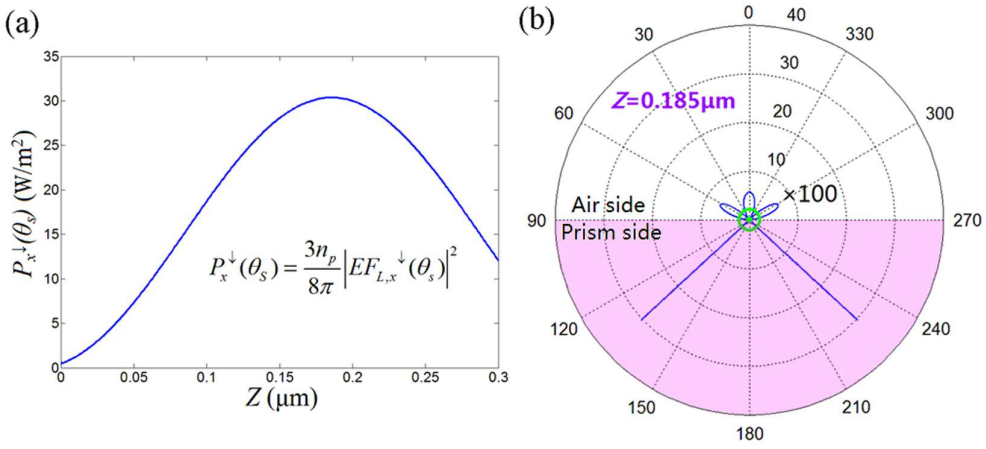

Fig. 5 (a) Power density of the TE-mode-coupled directional Raman emission from the x-oriented dipole confined in the core layer versus the distance *Z*; (b) Angular distribution of Raman power density from the x-oriented dipole located at *Z* = 0.185μm (the power density on the air-clad side is multiplied by 100 for a clear view).

For the Raman dipole oriented parallel to the y-axis, the electric field enhancement factor should be:

$$EF_{L,y}^{\downarrow,\uparrow}(\theta,Z)=\left|\frac{t_p^{\downarrow,\uparrow}}{t_{p1}^{\downarrow,\uparrow}}(1-r_{p1}^{\downarrow,\uparrow})\cos\theta_2\right| \tag{14}$$

$t_p^{\uparrow}$ is the TM-polarized electric field transmission coefficient from the core/air interface to the prism/gold interface, which has the opposite direction compared with $t_p^{\downarrow}$. $t_{p1}^{\uparrow}$ and $r_{p1}^{\uparrow}$ represent the TM-polarized electric field transmission coefficient and reflection coefficient from the dipole's

location to the prism/gold interface, respectively. $t_{p1}^{\downarrow}$ and $r_{p1}^{\downarrow}$ are similar to $t_{p1}^{\uparrow}$ and $r_{p1}^{\uparrow}$ except for the different direction, which is from the dipole's location to the core/air interface. θ_2 is the refraction angle in the core layer. In this situation, the directional emission angle could be the TM–mode resonance angle or the SPR mode resonance angle (θ_{spr}=59.54°). Fig. 6(a) shows the TM-mode-coupled directional power density as a function of the distance Z: the power density along the TM-mode resonance angle (θ_p=37.95°) initially increases with Z, reaching the maximum value of 4.82W/m^2 at Z=0.1μm, then decreases to nearly zero at Z=0.235μm and then increases to 2.16W/m^2 at Z=0.3μm. Fig. 6(b) illustrates the relationship between the SPR-mode-coupled directional power density and the distance Z: the directional power density simply decreases as Z increases and the maximum value is 0.57W/m^2 at Z=0. This is because the SPR mode is supported by the gold/core interface and the coupling efficiency is directly related to the distance between the dipole and this interface. Fig. 6(c) and 6(d) display the radiation patterns with Z=0.1μm and Z=0. The light in the prism side propagates along a single angle of θ_p in Fig. 6(c) and along the two angles θ_p and θ_{spr} in Fig. 6(d). The insets in Fig. 6(d) are the magnified views, showing that either the TM-mode-coupled or SPR-mode-coupled directional emission forms a slightly divergent beam with the largest intensity exactly at the resonance angle of the corresponding mode and that the angle divergence with the TM mode is much smaller than that with the SPR mode. The findings reveal that the guided-mode-coupled directional Raman emission has a lower divergence relative to that associated with SPR.

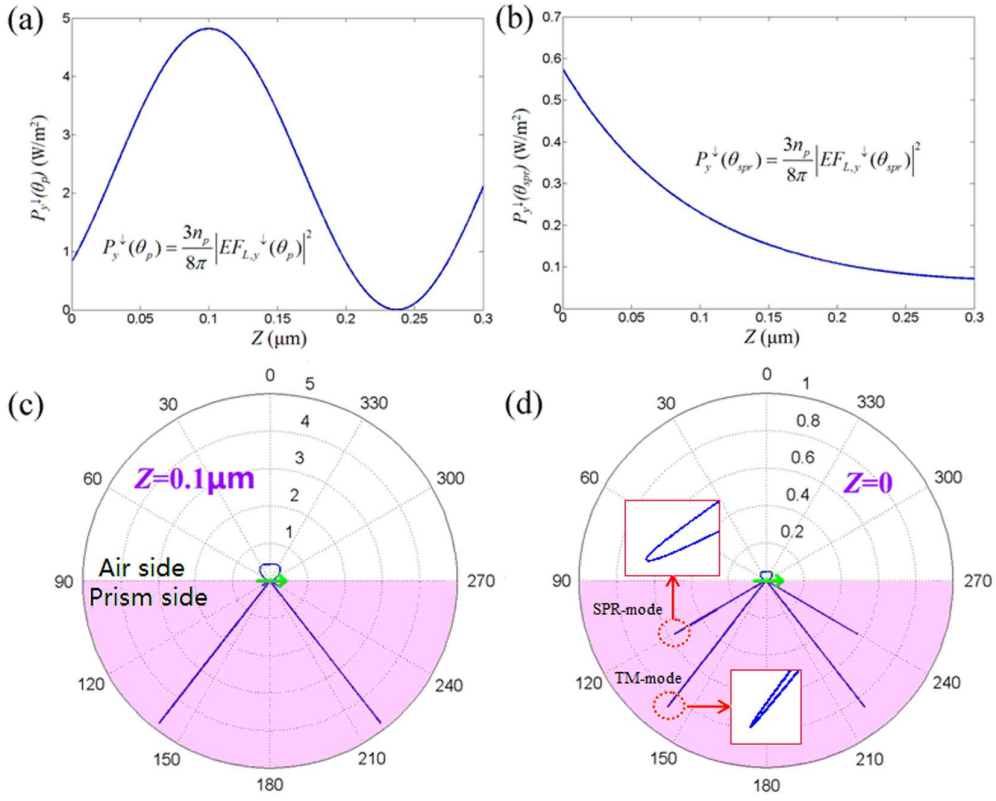

Fig. 6 Power densities of (a) the TM-mode-coupled (θ_p=37.95°) and (b) the SPR-mode-coupled (θ_{spr}=59.54°) directional Raman emissions from the y-oriented dipole versus the distance Z; Angular distributions of Raman power density from the y-oriented dipole located at (c) Z = 0.1μm and (d) Z = 0 [the insets in (d): the magnified view revealing

that the angle divergence for the TM-mode-coupled directional emission is much smaller than that for the SPR-mode-coupled directional emission.].

For the z-oriented Raman dipole, the electric field enhancement factor should be:

$$EF_{L,z}{}^{\downarrow,\uparrow}(\theta,Z)=\left|\frac{t_p{}^{\downarrow,\uparrow}}{t_{p1}{}^{\downarrow,\uparrow}}(1+r_{p1}{}^{\downarrow,\uparrow})\sin\theta_2\right| \tag{15}$$

The relationship between the TM-mode-coupled directional power density and the distance Z is shown in Fig. 7(a). The strongest directional power density of 5.99W/m^2 is obtained with Z=0.235μm and this value is 49 times larger than the maximum power density emitted in free space. Fig. 7(b) shows that the SPR-mode-coupled directional power density decreases as Z increases and the maximum value is 6.14W/m^2, which is 51 times larger than the maximum power density emitted in free space. Fig. 7(c) and 7(d) are the radiation patterns with Z=0.235μm and Z=0, respectively.

The simulation results in this section suggest that a higher Raman collection efficiency could be achieved by embedding the target molecules in the core layer but it strongly depends on both orientations and positions of the molecules.

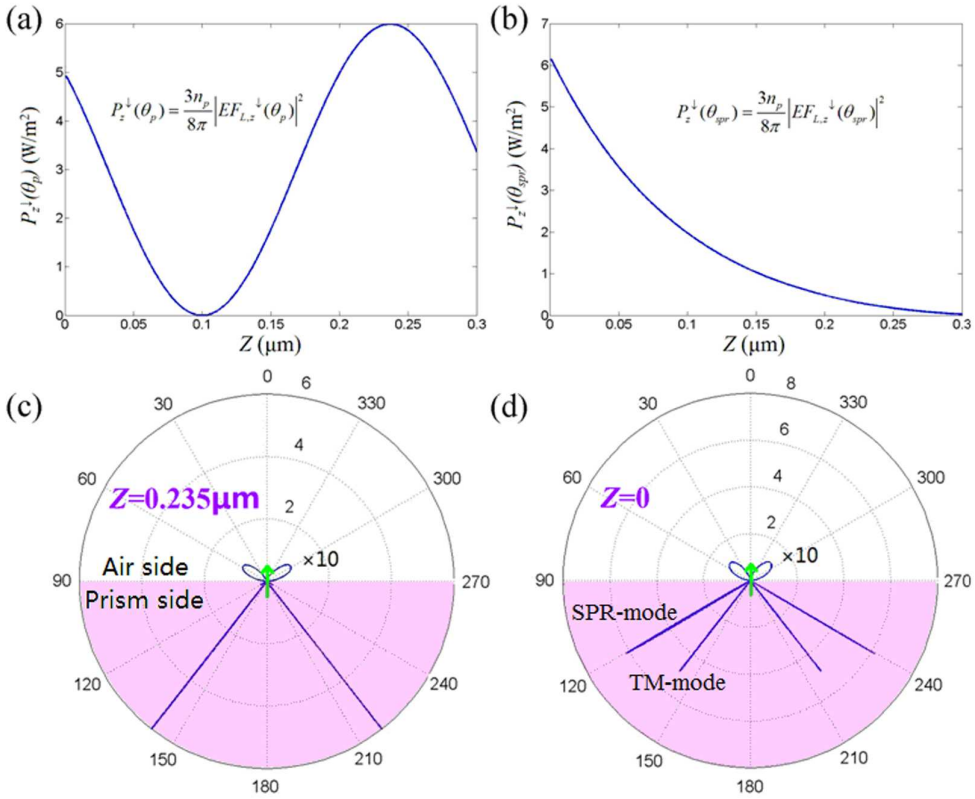

Fig. 7 Power densities of (a) the TM-mode-coupled and (b) the SPR-mode-coupled directional Raman emissions from the z-oriented dipole versus the distance *Z*; Angular distributions of Raman power density from the z-oriented dipole located at (c) *Z* = 0.235μm and (d) *Z* = 0 [the power densities on the air-clad side in (c) and (d) are multiplied by 10 for a clear view].

2.3. Raman enhancement factor with PW

The formulae mentioned above can also be used to calculate the spatial distribution of the field enhancement factor with a specific mode in a waveguide. The simulation results indicate that the field enhancement factor with the TE mode in a PW is larger than that with the TM mode in the same PW. Fig. 8 displays the TE-field enhancement factor profile with the PW shown in Fig. 1. The field enhancement factor on the PW surface (Z = 0.3μm) is EF_{field} = 7.5, corresponding to the directional Raman enhancement factor of $EF_{Raman} = 3\times10^3$ since it is proportional to the fourth power of the electric field enhancement factor [namely, $EF_{Raman}=(EF_{field})^4$]. The maximum field enhancement factor of EF_{field} = 12 appears in the core layer with Z=0.185μm, corresponding to the directional Raman enhancement factor of $EF_{Raman} \approx 2\times10^4$.

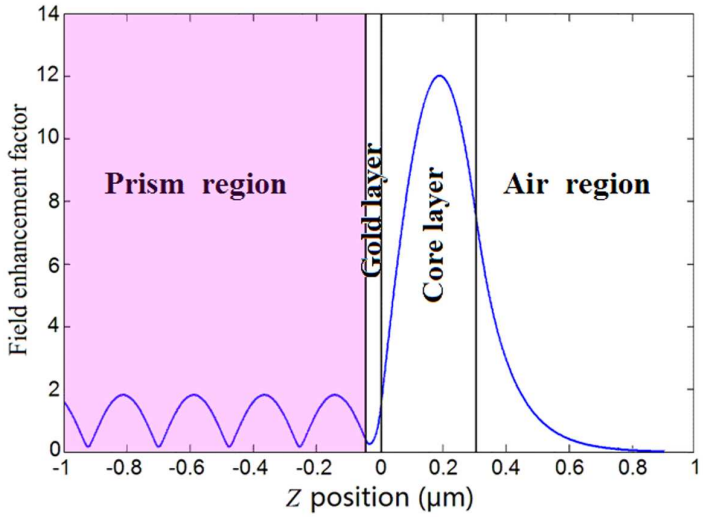

Fig. 8 Field enhancement factor profile with the TE mode in the PW.

3. Radiation pattern of Raman dipole with RM

Similar to the PW structure shown in Fig. 1, RM is also a four-layer structure with use of a low-index dielectric layer instead of the gold film in the PW. Simulations with the RM were performed using the same formulae mentioned above. The parameters of the RM structure used for simulation include: the prism index of n_p = 1.52, the buffer-layer thickness of 1250nm and its index of 1.38 (corresponding to MgF_2), the core-layer thickness of D_w = 250nm and its index of n_w = 1.49; the air-clad index of n_c =1. The radiation wavelength of Raman dipole is given as λ = 532nm and the distance between Raman dipole and buffer/core interface is denoted by Z.

3.1. Raman dipole located above the core layer

With Raman dipole located above the RM surface, the coupling efficiency between the radiation power and the resonance modes decreases as the distance Z increases just like the PW case and thus only the radiation patterns with $Z=D_w$ and $Z=D_w+\lambda$ are presented. For the x-oriented Raman dipole, Fig. 9(a) shows that the maximum Raman power density along the TE-mode resonance angle of θ_{sr}=67° is 326W/m^2, about 2716 times larger than the maximum power density emitted by the Raman dipole in free space. When Z increases to $D_w+\lambda$, the radiation along θ_{sr} is too weak to be observed according to Fig. 9(b). However, part of the radiation power is coupled into the TE-polarized leaking modes, which is directionally emitted in the critical angle of $\theta_c=asin(1/1.52)$=41.14° with an intensity of 1W/m^2. For the y-oriented Raman dipole, it is shown

by Fig. 9(c) that the maximum Raman power density along the TM-mode resonance angle of θ_{pr}=65.8° is 20.9W/m^2. The disappearance of directional emission is observed with $Z=D_w+\lambda$ as shown in Fig. 9(d). For the z-oriented Raman dipole, it is shown in Fig. 9(e) that the maximum Raman power density along θ_{pr}=65.8° is 43.5W/m^2. According to Fig. 9(f), the radiation along θ_{pr}=65.8° also disappears with $Z=D_w+\lambda$ and part of the radiation power is coupled into the TM-polarized leaking modes, which is directionally emitted in the critical angle of θ_c with an intensity of 1.62W/m^2. In conclusion, the directional emission along θ_c has no big influence on using this structure for interfacial Raman measurements owing to not only the angle difference but also the much weaker radiation intensity compared with that along θ_{sr} or θ_{pr}. It is obvious that the directional emission intensities with different oriented dipoles in the RM structure are larger than those in the PW structure: the absorption of metal material is avoided and a higher quality factor can be achieved with RM.

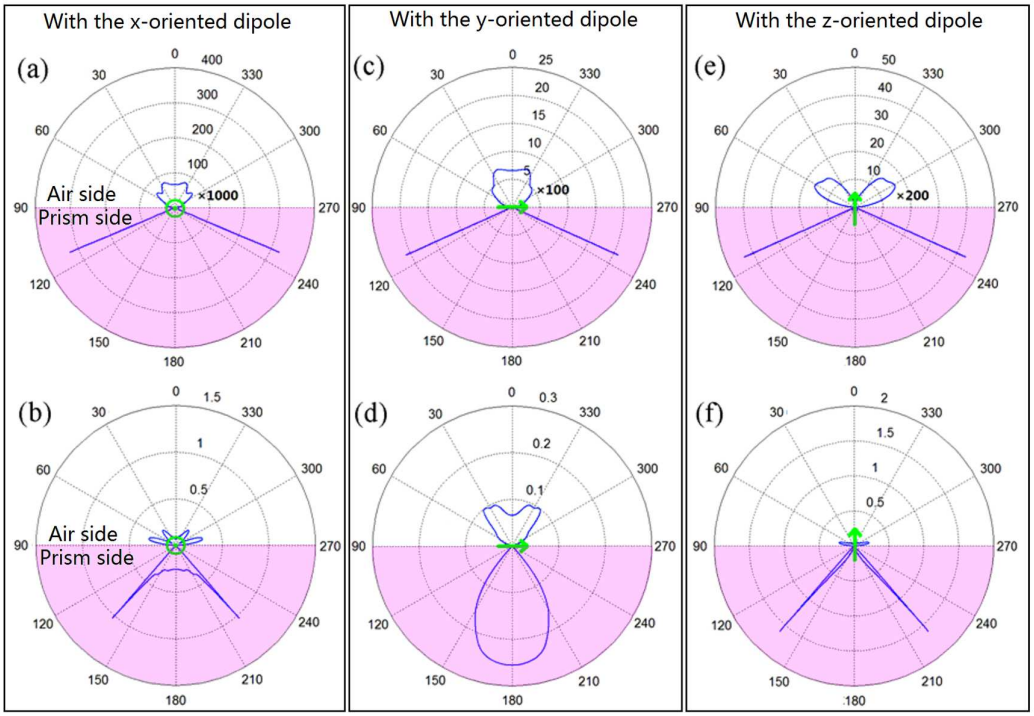

Fig. 9 Simulation results with the RM structure [(a) $Z= D_w$ and (b) $Z=D_w+\lambda$ with the x-oriented dipole; (c) $Z= D_w$ and (d) $Z=D_w+\lambda$ with the y-oriented dipole; (e) $Z= D_w$ and (f) $Z=D_w+\lambda$ with the z-oriented dipole].

3.2. Raman dipole located in the core layer

For the x-oriented Raman dipole, Fig. 10(a) shows the TE-mode-coupled directional power density as a function of the distance Z. It is worth noting that the coupling efficiency is always *higher* than that with Raman dipole located on the RM surface. The radiation pattern with Z=0.08μm is shown in Fig. 10(b) and the maximum power density is 1500W/m^2, about 12500 times larger than the maximum power density emitted in free space.

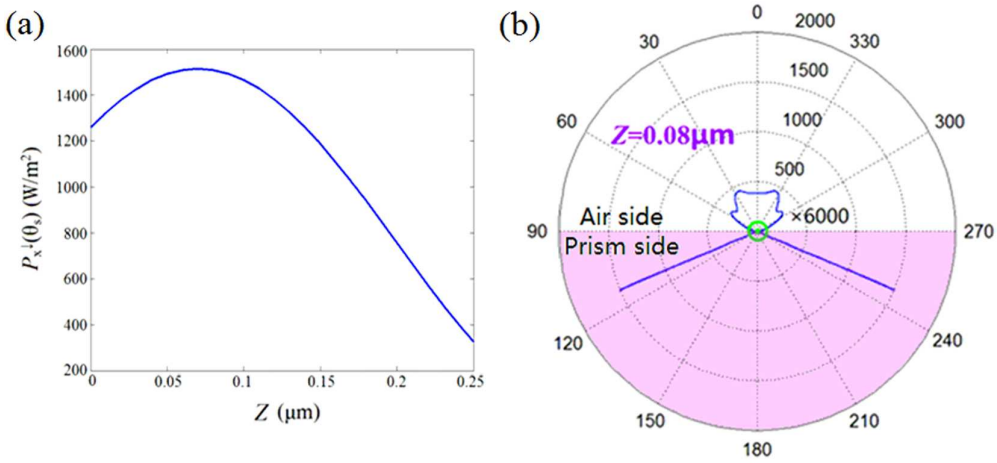

Fig. 10 (a) Power density of the TE-mode-coupled directional Raman emission from the x-oriented dipole confined in the core layer versus the distance *Z*; (b) Angular distribution of Raman power density from the x-oriented dipole located at *Z* = 0.08μm (the power density on the air-clad side is multiplied by 6000 for a clear view).

The relationship between the TM-mode-coupled directional power density and the distance *Z* was simulated with the Raman dipole oriented parallel to the y-axis. As shown in Fig. 11(a), the coupling efficiency is always smaller than that with dipole located on the RM surface. The angular distribution of Raman power density with *Z*=0.25μm is given by Fig. 11(b) and the maximum value is 20.9W/m^2. It's the same with Raman dipole located on the RM surface. This is because of the electric field continuity. For the Raman dipole oriented parallel to the z-axis, the maximal TM-mode-coupled directional power density is 143.6W/m^2 with *Z*=0.05μm, about 1196 times larger than the maximum power density emitted in free space. In the range of 0 ≤*Z*< 0.21μm, the coupling efficiency is larger than that with dipole located on the RM surface. The results are shown in Fig. 12(a) and 12(b).

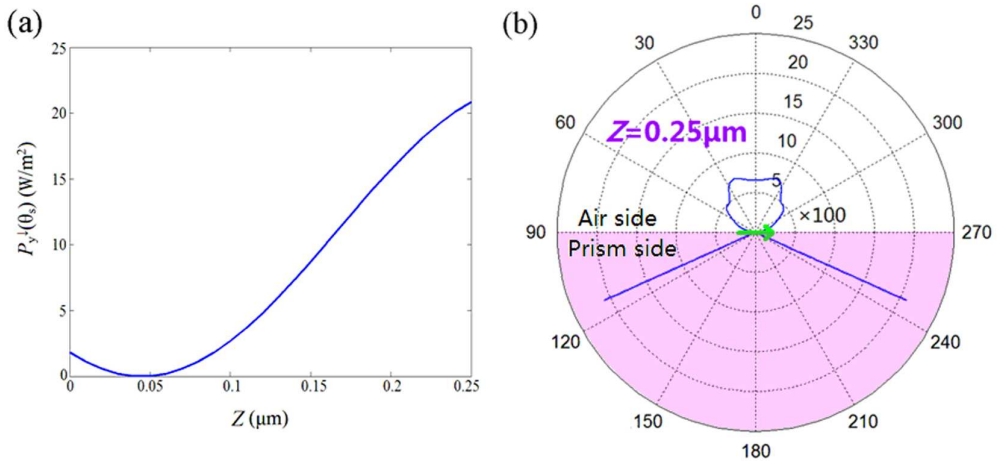

Fig. 11(a) Power density of the TM-mode-coupled directional Raman emission from the y-oriented dipole confined in the core layer versus the distance *Z*; (b) Angular distribution of Raman power density from the y-oriented dipole located at *Z* = 0.25μm (the power density on the air-clad side is multiplied by 100 for a clear view).

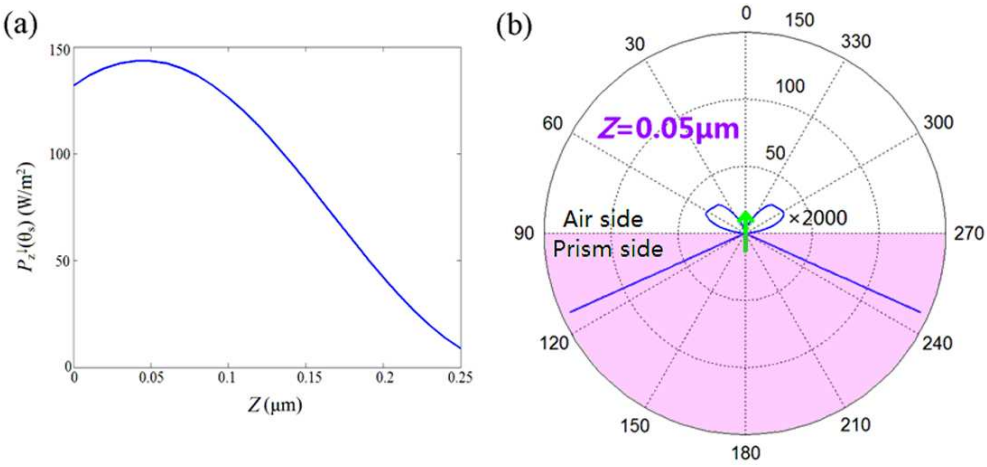

Fig. 12 (a) Power density of the TM-mode-coupled directional Raman emission from the z-oriented dipole confined in the core layer versus the distance *Z*; (b) Angular distribution of the Raman power density from the z-oriented dipole located at *Z* = 0.05μm (the power density on the air-clad side is multiplied by 2000 for a clear view).

3.3. Raman enhancement factor with RM

Similar to the simulation results with the PW structure, the TE-polarized light brings a higher field enhancement factor with RM, too. The field enhancement factor distribution with the TE mode is shown in Fig. 13. The field enhancement factor on the surface of the core layer is EF_{field}= 42.38, corresponding to the directional Raman enhancement factor of $EF_{Raman} \approx 3.2\times10^{6}$. The mode confinement in the core layer results in the maximum field enhancement factor of EF_{field}= 91.38 at the position of Z = 0.08μm, and the corresponding directional Raman enhancement factor is $EF_{Raman} \approx 7\times10^{7}$.

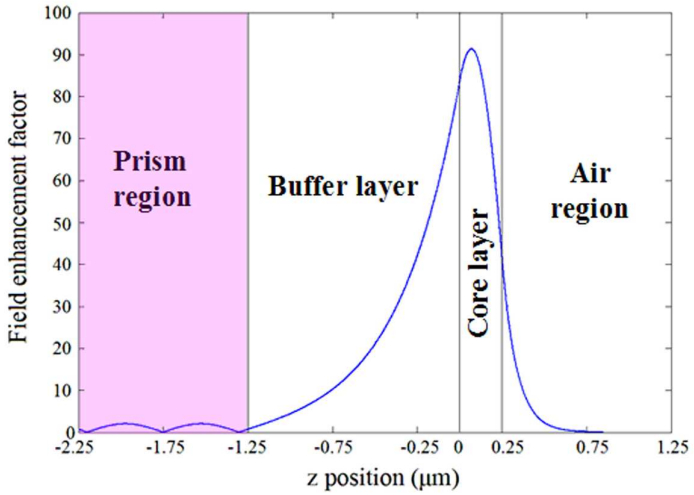

Fig. 13 Field enhancement factor profile with the TE mode in the RM.

4. Conclusion

In this work, the guided-mode-coupled directional Raman emission characteristics with the

PW and RM structures are theoretically investigated by the combination of the Fresnel equations and the optical reciprocity theorem. According to the different locations of the Raman dipole in the field-occupied region of the waveguide, the simulation results can be summarized as follows: (1) The directional Raman emission from a dipole located in the mode-occupied space heavily depends on both the dipole's orientation and its distance to the waveguide surface; (2) For a Raman dipole located above the waveguide surface, the coupling efficiency between the radiation power of the dipole and the guided modes decreases rapidly with increasing the distance; (3) A combination of the guided-mode excitation and the guided-mode-coupled directional emission makes the Raman power density decrease four times as fast as the evanescent field attenuation with increasing the distance, and this property offers the waveguide based directional Raman technique an outstanding depth resolution (in other words, this technique has the excellent surface selectivity); (4) With the RM structure the radiation power can also be coupled into the leaky modes in addition to the guided modes, and the light emitted via the leaky-mode coupling, however, has a great divergence and extremely weak intensity; (5) Immobilization of target molecules in the core layer of a single-mode waveguide can enhance the guided-mode-excited and guided-mode-coupled directional Raman emission; (6) A combination of the strong directivity and the lower divergence for the guided-mode-coupled Raman emission with the PW and RM structures is conducive to high-efficiency signal collection. It is worth noting that the method described in this work is also beneficial to the surface fluorescence spectroscopy and the single photon detection.

ACKNOWLEDGMENT

This work was supported by the National Basic Research Program of China (No. 2015CB352100), the Major National Scientific Instrument and Equipment Development Project of China (2011YQ0301240802), the National Natural Science Foundation of China (No. 61377064), and the Beijing Natural Science Foundation (No. 3131001).

Reference

[1] S. Nie, S. R. Emory, *Science*, 1997, 275, 1102-1106.
[2] K. Kneipp, Y. Wang, H. Kneipp, L. T. Perelman, I. Itzkan, R. R. Dasari and M. S. Field, *Phys. Rev. Lett.*, 1997, 78, 1667-1670.
[3] B. L. Darby, P. G. Etchegoin and E. C. Le Ru, *Phys. Chem. Chem. Phys.*, 2014, 16, 23895-23899.
[4] H.M. Lee, S. M. Jin, H. M. Kim and Y. D. Suh, *Phys. Chem. Chem. Phys.*, 2013, 15, 5276-5287.
[5] Z. Q. Tian, B. Ren, B. W. Mao, *J. Phys. Chem. B*, 1997, 101, 1338-1346.
[6] M. Moskovits, *Reviews of Modern Physics*, 1985, 57, 783-826.
[7] E. C. Le Ru, P. G. Etchegoin, *Chemical Physics Letters*, 2006, 423, 63-66.
[8] S. Y. Ding, D. Y. Wu, Z. L. Yang, B. Ren, X. Xu, Z. Q. Tian , *Chemical Journal of Chinese Universities*, 2008, 29, 2569-2581.
[9] L. D'Hooge, J. M. Vigoureux, *Chemical Physics Letters*, 1979, 65, 500-506.
[10] K. J. McKee, M. W. Meyer, E. A. Smith, *Anal. Chem.*, 2012, 84, 4300-4306.
[11] Y. Liu, S. Xu, B. Tang, Y. Wang, J. Zhou, X. Zheng, B. Zhao, W. Xu, *Review of Scientific Instruments*, 2010, 81, 036105.
[12] S. A. Meyer, B. Auguié, E. C. Le Ru, P. G. Etchegoin, *J. Phys. Chem. A*, 2012, 116, 1000-1007.
[13] S. A. Meyer, E. C. Le Ru, P. G. Etchegoin, *Anal. Chem.*, 2011, 83, 2337-2344.
[14] K. J. McKee, M. W. Meyer, E. A. Smith, *Anal. Chem.*, 2012, 84, 9049-9055.
[15] D. B. Hu, C. Chen, Z. M. Qi, *J. Phys. Chem. C*, 2014, 118, 13099-13106.
[16] D. B. Hu, Z. M. Qi, *J. Phys. Chem. C*, 2013, 117, 16175-16181.
[17] W. Lukosz, *J. Opt. Soc. Am.*, 1977, 69, 1495-1503.
[18] T. H. Taminiau, F. D. Stefani, F. B. Segerink, N. F. Van Hulst, *Nat. Photonics*, 2008, 2, 234-237.
[19] K. G. Lee, X. W. Chen, H. Eghlidi, P. Kukura, R. Lettow, A. Renn, V. Sandoghdar and S. Götzinger, *Nat. photonics*, 2011, 5, 166-169.
[20] J. R. Lakowicz, *Analytical Biochemistry*, 2004, 324, 153-169.
[21] Q. Zhao, D. F. Lu, D. L. Liu, Z. M. Qi, *Acta Physico-Chimica Sinica*, 2014, 30, 1201-1207.
[22] H. Li, S. Xu, Y. Liu, Y. Gu, W. Xu, *Thin Solid Films*, 2012, 520, 6001-6006.
[23] F. Masayuki, M. Satoshi, *Analytical Sciences/Supplements*, 2002, 17icas, i103.
[24] C. Remi, N. V. Manuel, *J. Opt. Soc. Am.*, 1998, 15, 706-712.
[25] J. D. Jackson, *Classical Electrodynamics*, John Wiley& Sons, INC, 3nd edn., 1998, ch.9, pp.410-413.
[26] I. Gryczynski, J. Malicka, Z. Gryczynski and J. R. Lakowicz, *Analytical Biochemistry*, 2004, 324, 170-182.
[27] M. Born, E. Wolf, *principles of optics*, Cambridge university press, 7nd edn., 1999, ch.1, pp.38-70.
[28] M. C. Marco de Lucas, B. Jacquier, E. Lebrasseur, J. Y. Rivoire, *Review of Scientific Instruments*, 1997, 68, 2275-2278.
[29] S. B. Ellahi, R. E. Hester, *Anal. Chem.*, 1995, 67, 108-113.